ASSESSMENT OF SOLAR RESOURCE AVAILABILITY AND ITS CLIMATIC DRIVERS AT A REPRESENTATIVE GRID POINT IN THE GAMBIA

Bubacarr Jawla[1], Faye Jerreh Manneh[2], Sherif A Bah[3], Omar M Camara[4], Sainey Danjo[5], Modou Lamin Trawally[6]

[1]Natural Resources and Environmental Engineering Study Program (Postgraduate), Department of Biosystem Engineering, Faculty of Agro-Industrial and Biosystems Technology, Universitas Brawijaya, Malang, Indonesia
[2]Department of Crop Protection, Faculty of Agriculture and Environmental Sciences, University of The Gambia, Faraba, Banjul, Gambia
[3]Department of Mathematics, Faculty of Mathematics and Natural Sciences (FMIPA), Universitas Brawijaya, Malang, Indonesia
[4]Department of Agro-industrial Technology, Faculty of Agro-Industrial and Biosystems Technology, Universitas Brawijaya, Malang, Indonesia
[5]Department of Plant Pathology, Faculty of Agriculture, Universitas Brawijaya, Malang, Indonesia
[6]Graduate Education Institute, Faculty of Agriculture, Yozgat Bozok University, Yozgat, Turkey

E-mail: bubacarrjawla@student.ub.ac.id

Received: July 18, 2026 | **Accepted:** September 25, 2026 | **Published:** September 26, 2026
DOI: 10.12962/j27745449.v6i3.10582 | **Issue:** Volume 6 Number 3 2025 | E-ISSN: 2774-5449

ABSTRACT

Assessment of long-term solar resource variability and its climatic controls is essential for sustainable photovoltaic deployment in data-scarce regions. This study evaluated solar resource availability and its climatic drivers at a representative central grid point in The Gambia (13.45° N, 15.38° W) using monthly NASA POWER satellite- and reanalysis-derived estimates from 1998 to 2025. Solar radiation (All-sky surface shortwave (solar) downward irradiance), Clear-sky surface shortwave downward irradiance, cloud cover, air temperature, specific humidity, wind speed, and precipitation were analyzed using descriptive climatology, clear-sky index assessment, Mann-Kendall trend analysis, correlation analysis, and multiple linear regression on both raw and deseasonalized datasets. The results showed that solar resource availability was consistently high during the dry season (November to May), with clear sky index values ranging from 0.90 to 0.96, whereas atmospheric transmissivity was markedly lower during the monsoon season, reaching a low of 0.760 in August. Long-term trend analysis revealed no statistically significant change in solar radiation over the research period, despite minor drops in August and September. After adjusting for seasonal impacts, cloud quantity emerged as the most important predictor of solar radiation fluctuation. Simultaneously, the apparent positive correlations between temperature and wind speed reflected shared seasonal cycles rather than direct physical controls. These findings highlight The Gambia's substantial and seasonally variable solar irradiance resource and indicate cloud fluctuation as the primary atmospheric restriction for solar resource assessment, photovoltaic planning, operational forecasting, and climate-resilient energy policy, providing a point-scale baseline for future multi-site assessment across the country.

Keyword: Solar resource assessment, Climatic drivers, clear sky index, Solar irradiance variability, NASA POWER

Introduction

The worldwide shift to sustainable energy systems has expedited the development of renewable energy technologies, as nations work to lower greenhouse gas emissions, enhance energy security, and meet climate mitigation goals [1]. Owing to its availability, environmental friendliness, and decreasing installation prices, solar energy has emerged as one of

the fastest-growing renewable energy sources with the quickest rate of growth [2]. However, the availability of solar radiation, which is affected by both atmospheric and astronomical circumstances, is the main factor determining the dependability and efficiency of solar energy systems [2]. Therefore, maximizing photovoltaic system efficiency, enhancing energy forecasting, and bolstering evidence-based renewable energy planning all depend on understanding the temporal variability of solar radiation and the climatic conditions influencing its availability [3].

Sub-Saharan Africa has some of the highest solar energy potential in the world because of its tropical position and high annual solar irradiation. The Gambia is especially well-suited for solar energy development in the region because of its ample sunshine and rising demand for dependable electricity

However, the nation's energy sector is still heavily reliant on imported fossil fuels, which raises the cost of producing electricity and makes it susceptible to changes in international fuel markets [4]. The Gambia's government has made the development of renewable energy a top priority as part of its plan to increase electricity availability and lower carbon emissions after realizing these difficulties. Accurate long-term evaluations of solar resource availability and a deeper comprehension of how climate variability affects solar energy potential are necessary for the successful execution of these efforts [5].

In addition to the Earth's position relative to the sun, atmospheric factors, such as cloud cover, humidity, precipitation, temperature, and wind speed, also influence surface solar radiation [6]. The quantity of solar energy that reaches the Earth's surface is determined by these factors, which also affect the transmission, absorption, and scattering of incoming solar radiation [7]. Clear skies increase solar energy availability; however, increased cloud cover and air moisture typically decrease solar irradiance [8]. Similarly, variations in solar radiation throughout the year are influenced by seasonal changes in air circulation and precipitation [9]. Evaluating these interactions has become more crucial for enhancing the assessment of solar resources and guaranteeing the long-term dependability of solar energy systems as climate unpredictability increases [10].

Previous research has comprehensively evaluated solar energy resources using satellite observations and ground-based measurements. These studies consistently reveal that tropical locations have a high solar energy potential but also experience significant seasonal and interannual fluctuations caused by atmospheric processes [11]. According to research, cloud cover is one of the most effective restrictions on surface solar radiation. Temperature, humidity, precipitation, and wind speed all influence solar resource availability by affecting air transparency and cloud formation [12]. Several West African studies have used statistical and modelling approaches to study the links between solar radiation and climatic variables, finding that incorporating several meteorological elements increases the accuracy of solar resource assessment and prediction [13,14].

Despite these advances, research focusing specifically on The Gambia remains limited. Most existing studies have concentrated on estimating average solar irradiation or evaluating the technical feasibility of photovoltaic systems, with limited attention given to long-term trends, seasonal variability, and the combined influence of multiple climatic variables [15]. Furthermore, very few studies have isolated the weather-scale (intra-seasonal) influence of climatic drivers on solar radiation from the shared seasonal cycle that both follow, because temperature, humidity, cloud cover, wind speed, and precipitation all track the same annual rainfall-driven cycle in this region. Raw-value correlations and regressions risk overstating the physical coupling between them. Second, a statistical gap exists: studies that test for solar radiation trends on a monthly or seasonal basis typically run several independent significance tests, such as one per calendar month, without correcting for the resulting increase in the chance of a false-positive finding; thus, apparent significant trends may not survive scrutiny once multiple comparisons are properly accounted for. The third gap is the near-absence, specifically for The Gambia, of a systematic comparison between measured (all-sky) and theoretical (clear-sky) surface solar radiation. Such a comparison, expressed as a clear-sky index, isolates atmospheric attenuation from the astronomically driven component of solar radiation and has not been quantified at a monthly, multi-decadal resolution for the country. Addressing these three gaps, namely disentangling seasonal from weather-scale drivers, guarding against multiple-testing error inflation, and quantifying atmospheric attenuation through an all-sky-clear-sky comparison, is crucial for more effective planning for renewable energy in The Gambia and for

guiding climate-resilient energy policy development in the future.

Accordingly, the purpose of this study was to assess the long-term trends and temporal characteristics of solar irradiance availability at a representative central grid point in The Gambia from 1998 to 2025 and to determine the seasonal and interannual variability of solar radiation at this location. This study addresses these three gaps directly and, in doing so, makes three specific methodological contributions to The Gambian and West African solar resource literature. First, it constructs a parallel de-seasonalized (anomaly) dataset for all seven variables, obtained by removing the calendar-month climatological mean from each series, so that correlation, trend, and regression analyses can distinguish climatic associations that are artifacts of the shared seasonal cycle from those that persist at the weather (intra-seasonal) scale, a distinction that previous single-site Gambian assessments have not drawn. Second, it applies the Benjamini-Hochberg false discovery rate procedure and the Bonferroni correction to the twelve calendar-month Mann-Kendall trend tests, reporting adjusted alongside raw p-values so that any claimed long-term trend is robust to the multiple-testing problem inherent in month-by-month analysis, rather than relying on uncorrected significance as prior regional studies have generally done. Third, it computes a monthly clear-sky index (Kc = ALLSKY_SFC_SW_DWN / CLRSKY_SFC_SW_DWN) across the full 28-year record, providing a systematic all-sky-to-clear-sky comparison for a Gambian grid point, thereby isolating atmospheric transmissivity losses, which are cloud- and aerosol-driven, from the astronomically determined component of solar radiation. Together, these three methodological elements, namely anomaly-based separation of seasonal and weather-scale signals, multiple-testing-corrected trend detection, and a quantified all-sky/clear-sky comparison, constitute the novelty of this study and distinguish it from earlier Gambian and West African solar resource assessments, which have typically reported uncorrected trends and raw-value associations without separating these two temporal scales or benchmarking against the clear-sky envelope. Combined with a 28-year monthly record, this provides a new point-scale understanding of solar resource availability at a representative location in The Gambia, offering a methodological template and empirical baseline against which future multi-site assessments across the country can be compared.

Methodology

Study Area

The Republic of The Gambia, in the Sahelo-Sudanian transition zone of West Africa (approximately 13.0°–13.8° N, 13.8°–16.8° W), was adopted as the study domain. The narrow, elongated geography, low elevation (<30 m a.m.s.l.), and coastal proximity result in a tropical climate with a unimodal rainy season (June–October) associated with the seasonal migration of the Inter-Tropical Convergence Zone (ITCZ) and a long dry season (November–May) marked by the presence of the Saharan Harmattan. The Gambia is in the Sub-Saharan high insolation belt and is an important but understudied case for solar resource studies. The investigations focused on a representative grid point located at 13.45° N and 15.38° W, which represents the central point of The Gambia. The country is latitudinally small (< 1°) and is therefore assumed to have low monthly climate fluctuations; the location of the representative grid point is shown in Figure 1. Nonetheless, a single grid point cannot capture the full spatial variability of solar resource availability across the country, particularly the coastal-to-inland gradients in cloud cover, humidity, and Harmattan-driven aerosol loading. The results reported below therefore characterize solar resource conditions at this specific central location and are presented as a single-site (point-scale) assessment rather than as a spatially exhaustive national characterization.

Data Source and Acquisition

Climate data for each month from January 1998 to December 2025 (n = 336 monthly observations per variable) were obtained from the NASA Prediction of Worldwide Energy Resources (POWER) database, Native Resolution Monthly and Annual product, via the POWER Data Access Viewer API. NASA POWER combines satellite and reanalysis estimates at 0.5° × 0.625° (~50-60 km) and has substantial validation for solar resource evaluation in data-scarce applications, such as West Africa, where ground-based pyranometric networks are scarce [16] (Quansah et al., 2022a). Seven parameters were retrieved for the study grid point at the local standard time resolution (Table 1).

The useable surface solar radiation, ALLSKY_SFC_SW_DWN, was the primary response variable, with the clear sky index calculated from CLRSKY_SFC_SW_DWN. CLOUD_AMT, T2M, QV2M, WS2M,

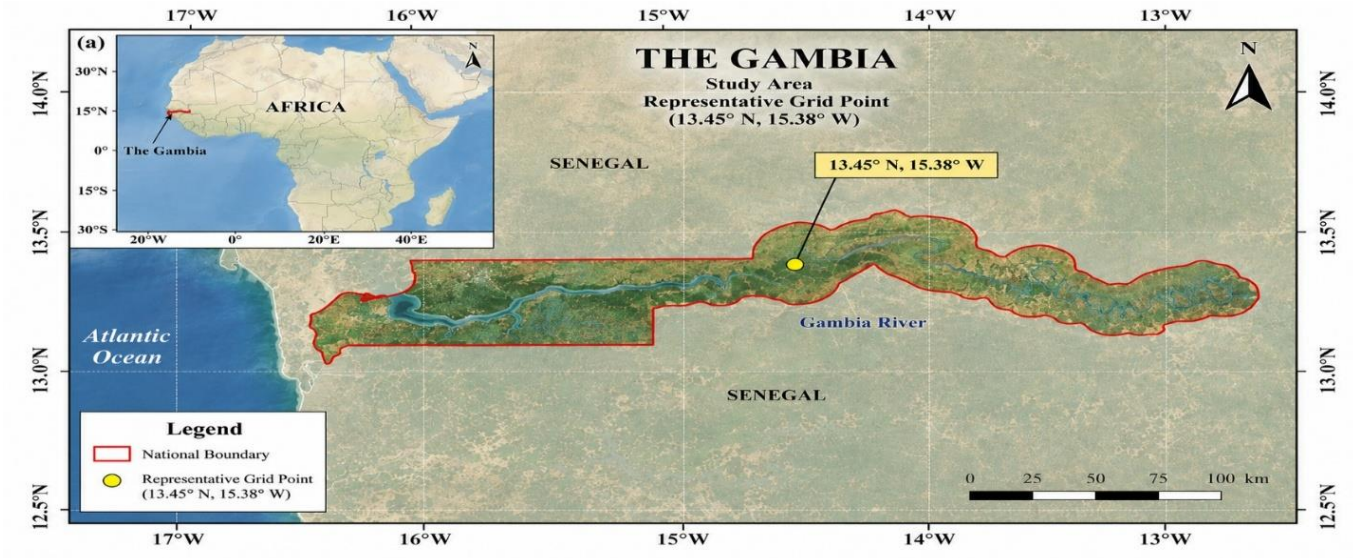


Figure 1. Location of the representative study grid point in the Republic of The Gambia, West Africa.

Table 1. NASA POWER climatic variables retrieved for the study grid point (13.45° N, 15.38° W), including variable code, description, source product, and unit of measurement.

Variable code	Description	Source	Unit
ALLSKY_SFC_SW_DWN	All-sky surface shortwave (solar) downward irradiance	CERES SYN1deg	MJ m^{-2} day^{-1}
CLRSKY_SFC_SW_DWN	Clear-sky surface shortwave downward irradiance	CERES SYN1deg	MJ m^{-2} day^{-1}
CLOUD_AMT	Cloud amount (cover fraction)	CERES SYN1deg	%
T2M	Air temperature at 2 m	MERRA-2	°C
QV2M	Specific humidity at 2 m	MERRA-2	g kg^{-1}
WS2M	Wind speed at 2 m	MERRA-2	m s^{-1}
PRECTOTCORR (IMERG_PRECTOT)	Bias-corrected total precipitation	MERRA-2 / IMERG	mm day^{-1}

and PRECTOTCORR were evaluated as variables for physical links to atmospheric transmissivity, specifically cloud attenuation, thermally driven stability, moisture loading, and boundary-layer mixing.

Data Quality Control and Preprocessing

NASA POWER's missing-value flag (−999) identified a single flagged satellite- and reanalysis-derived estimate (December 2025, CLOUD_AMT), which was excluded from the regression analyses, yielding n = 335 valid monthly satellite- and reanalysis-derived estimates; no other missing or flagged values were present in the retrieved series. Widely styled tables for each variable were reformatted into monthly time series and merged into a single analytical data frame using the YEAR-MONTH key. In this monsoonal climate, all six variables have a substantial annual cycle; therefore, any apparent link between solar radiation and climatic drivers is likely to be distorted by this cycle. These impacts were separated by constructing a parallel de-seasonalized (anomaly) dataset for each variable by subtracting the long-term climatological mean from all variables with the same calendar month, resulting in monthly anomalies that do not follow the seasonal cycle. Raw monthly values and deseasonalized anomalies were then used in subsequent correlation and regression analyses to distinguish seasonality from intra-seasonality or weather-scale connections.

Analytical Framework

The analytical process was divided into four complementary elements: (i) descriptive solar resource climatology using the clear sky index ; (ii) trend detection on a monthly timescale; (iii) bivariate correlation analysis; and (iv) multivariate regression modelling of climatic drivers, all of which were performed in Python 3.11.

Solar Resource Climatology and clear sky index

Monthly and annual descriptive statistics (mean, standard deviation, and coefficient of variation) were computed for ALLSKY_SFC_SW_DWN to describe the long-term solar resource climatology and intra-annual variability. To estimate the size and temporal stability of the atmospheric attenuation (mainly cloud- and aerosol-related losses) with respect to the "clear-sky" maximum, each calendar month of the 28-year record was analyzed for the monthly clear-sky index (Kc), a dimensionless measure of atmospheric transmissivity defined as Kc = ALLSKY_SFC_SW_DWN / CLRSKY_SFC_SW_DWN.

clear sky index (Kc)

$$Kc = H / Hcs \quad (1)$$

where H is the monthly mean all-sky surface solar irradiance (ALLSKY_SFC_SW_DWN), and Hcs is the monthly mean clear-sky surface solar irradiance (CLRSKY_SFC_SW_DWN). Kc is dimensionless and ranges from 0 (fully attenuated) to a theoretical maximum near 1 (unattenuated, clear-sky conditions).

Monthly Trend Analysis

Solar radiation anomalies were evaluated annually, but on a calendar monthly basis to eliminate the seasonal cycle and find month-specific trends that were not obvious in the yearly dataset. Three complementary estimators were used for each 28-year monthly sub-series: (i) ordinary least squares (OLS) linear regression against year; (ii) the non-parametric Mann-Kendall (MK) test [17], which is robust against non-normality and outliers; and (iii) the median-based rate of change, Theil-Sen slope estimator [18]. Twelve monthly tests were performed, and the raw p values were adjusted for multiple comparisons using the Benjamini-Hochberg false discovery rate procedure [19], and the more conservative Bonferroni correction, with adjusted p values reported alongside raw p values to avoid overreporting the Type 1 error rate.

Mann–Kendall Test and Sen's Slope

$$S = \Sigma_{i=1}^{n-1} \Sigma_{j=i+1}^{n} sgn(x_j - x_i) \quad (2)$$

$$Var(S) = [n(n-1)(2n+5) - \Sigma\, t_p(t_p-1)(2t_p+5)] / 18 \quad (3)$$

$$Z = (S-1)/\sqrt{Var(S)} \text{ if } S > 0;\ 0 \text{ if } S = 0;\ (S+1)/\sqrt{Var(S)} \text{ if } S < 0 \quad (4)$$

$$Q = median\{(x_j - x_i)/(j-i)\}, \text{ for all } i < j \quad (5)$$

Here, sign(θ) equals +1, 0, or −1 according to whether θ is positive, zero, or negative; x_i and x_j are the sequential annual values of a given calendar month's solar radiation series (i < j); n is the number of years in the sub-series (n = 28); t_p is the number of data points in the p-th group of tied values; and Q is the Theil–Sen estimator of the monthly trend magnitude, reported in W m^{-2} per year. The Mann–Kendall Z statistic (Eq. 4) is compared against the standard normal distribution to test the null hypothesis of no trend at α = 0.05. Raw p-values from the twelve-monthly tests were adjusted for multiple comparisons using the Benjamini–Hochberg false discovery rate procedure and the Bonferroni correction.

Correlation Analysis

The association between ALLSKY_SFC_SW_DWN and each climatic driver (T2M, QV2M, CLOUD_AMT, WS2M, PRECTOTCORR) was measured using the Pearson product-moment coefficient (linear association) and the Spearman rank coefficient (monotonic association, less sensitive to distributional departures). Both were calculated from (i) raw monthly values that contain the common seasonal signal, and (ii) de-seasonalized anomalies, where association due to intra-seasonal variability is separated from the association due to the annual cycle, eliminating some seasonally confounded relationships and highlighting others that persist outside of the annual cycle.

Pearson r and Spearman ρ

$$r = \Sigma(x_i - \bar{x})(y_i - \bar{y}) / \sqrt{[\Sigma(x_i - \bar{x})^2 \times \Sigma(y_i - \bar{y})^2]} \quad (6)$$

$$\rho = 1 - [6\Sigma d_i^2 / n(n^2 - 1)] \quad (7)$$

Here, x_i and y_i are the paired satellite and reanalysis-derived estimates of solar radiation and a given climatic driver, $\bar{x}$ and $\bar{y}$ are their means, d_i is the difference between the ranks of each paired satellite- and reanalysis-derived estimate, and n is the number of monthly satellite and reanalysis-derived estimates. Both r and ρ range from −1 (perfect negative association) to +1 (perfect positive association), with 0 indicating no linear (r) or monotonic (ρ) association. Both coefficients were computed from raw monthly values and from de-seasonalized anomalies to separate association driven by the shared annual cycle from association that persists at the intra-seasonal (weather) scale.

Multiple Linear Regression and Collinearity Diagnostics

Ordinary least-squares multiple linear regressions (OLS-MLR) were fitted with ALLSKY_SFC_SW_DWN as the dependent variable and T2M, QV2M,

CLOUD_AMT, WS2M, and PRECTOTCORR as the independent variables, using raw data and de-seasonalized anomalies separately. Unstandardized coefficients (beta), standardized coefficients, standard errors, and significance levels were reported; the standardized coefficients ranked the importance of the predictors on scales that were not commensurable. Multicollinearity was diagnosed by calculating the variance inflation factor (VIF) for each predictor [20], and the Durbin–Watson statistic [21] was used to test for first-order serial autocorrelation in the monthly climatic series, which is a common concern. The overall fit was evaluated using the coefficient of determination (R^2) and the F-statistic.

The value of R^2 indicates the explanatory power of the model from 0 (no explanatory power) to 1 (a perfect fit). Its value increases with the addition of predictors, irrespective of their explanatory power; hence, both the raw value of R^2 and the adjusted R^2, which emphasizes model simplicity, were reported and compared with the raw value and de-seasonalized anomaly model.

Importantly, a high R^2 does not establish physical causation or an artifact-free fit. Standard errors are biased by multicollinearity among predictors with a common seasonal cycle (e.g., specific humidity has the highest VIF at 7.67), and residual positive autocorrelation (Durbin–Watson = 1.02) is present, which can overestimate the explanations. In the de-seasonalized anomaly model, the R^2 drops to 0.438, all VIF values are below 1.7, and the Durbin–Watson statistic (1.53) is closer to the target value of 2, which means that the model is more statistically satisfactory and physically interpretable. The anomaly model R2 was thus considered a more meaningful measure of the true weather-scale predictive power of the climatic drivers.

$$Y = \beta_0 + \beta_1 T2M + \beta_2 QV2M + \beta_3 CLOUD_AMT + \beta_4 WS2M + \beta_5 PRECTOTCORR + \varepsilon \quad (8)$$

$$R^2 = 1 - (SS_res / SS_tot) \quad (9)$$

$$Adjusted\ R^2 = 1 - [(1 - R^2)(n - 1) / (n - k - 1)] \quad (10)$$

$$F = [R^2 / k] / [(1 - R^2) / (n - k - 1)] \quad (11)$$

$$VIF_j = 1 / (1 - R^2_j) \quad (12)$$

$$d = \Sigma (e_t - e_{(t-1)})^2 / \Sigma e_t^2 \quad (13)$$

Here, Y is the predicted surface solar radiation (ALLSKY_SFC_SW_DWN); β_0–β_5 are the unstandardized regression coefficients; ε is the residual error term; SS_res and SS_tot are the residual and total sums of squares, respectively; n is the number of monthly satellite and reanalysis-derived estimates used in the regression models after quality control (n = 335, following exclusion of the single flagged December 2025 CLOUD_AMT satellite and reanalysis-derived estimate; see Data Quality Control and Preprocessing); k is the number of predictors (k = 5); R^2_j is the coefficient of determination obtained when predictor j is regressed on the remaining predictors; and e_t is the regression residual at time t.

Software and Computational Environment

Data organization, processing, statistical analysis, and visualization were carried out in Python (v3.11) using the pandas and NumPy modules. We used OLS regression, Pearson-Spearman correlation, VIF, the Durbin-Watson test, and multiple-testing modules. The SciPy and statsmodels libraries were used to perform the Benjamini-Hochberg and Bonferroni tests, respectively, while the pymannkendall library was utilized for the Mann-Kendall test and Theil-Sen slope estimate. The accompanying climatological and diagnostic graphics were created using Matplotlib and Seaborn. We evaluated statistical significance using the standard criterion of $\alpha = 0.05$.

Result and Discussion

Solar Resource Climatology and Atmospheric Transmissivity

Mean monthly all-sky surface irradiance closely tracked the clear-sky envelope during the dry season (November–May) but diverged from it during the monsoon months (July–September) (Figure 2). The clear sky index (Kc, Table 2) was high and stable from November to May (Kc = 0.90–0.96; CV = 1.1–3.9%), but dropped markedly during the monsoon core, reaching a low of Kc= 0.760 (CV = 4.32%) in August, and remained low in July (Kc = 0.818) and September (Kc = 0.804), before increasing again in October (Kc = 0.900).

The coefficient of variation of Kc was, on average, about 40% higher during the monsoon season (June–October; CV = 2.7–4.8%) than during the dry season (November–May; CV = 1.1–3.9%), and more than quadrupled at its monsoon peak (September, CV = 4.76%) relative to the driest, most stable month (April, CV = 1.06%) (Table 2; Figure 3), showing that the monsoon season has both the lowest transmissivity and the highest month-to-month variation.

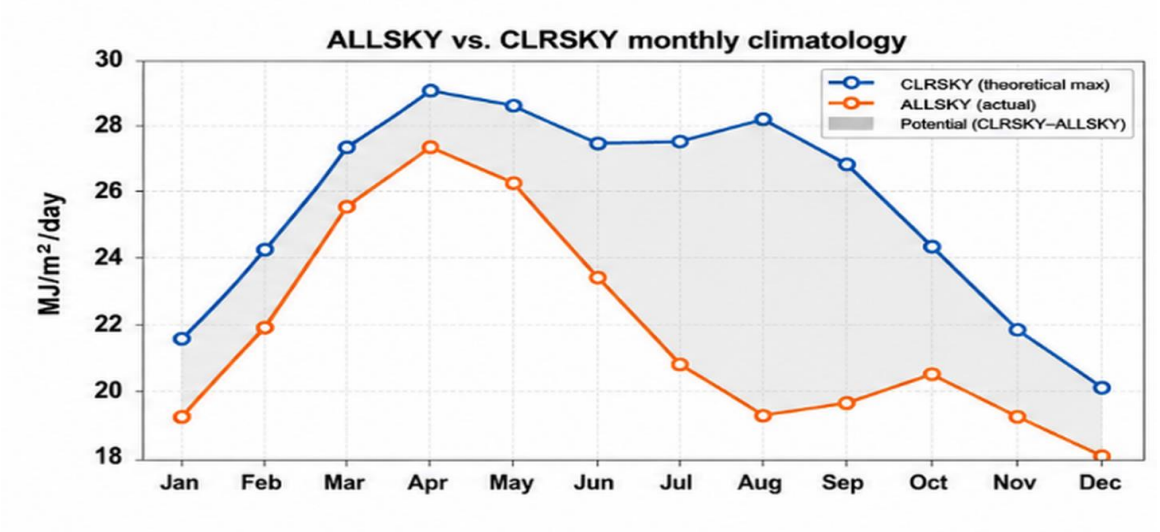


Figure 2. Monthly climatology of all-sky (actual) and clear-sky (theoretical maximum) surface solar irradiance at the study grid point, The Gambia, 1998–2025. The shaded band indicates the unrealized ("potential") solar resource, i.e., the gap between the clear-sky ceiling and the actual all-sky irradiance.

Table 2. Monthly clear sky index (Kc = ALLSKY_SFC_SW_DWN / CLRSKY_SFC_SW_DWN) climatology, 1998–2025.

Month	Mean Kc	SD	CV (%)
Jan	0.920	0.027	2.89
Feb	0.940	0.030	3.20
Mar	0.960	0.017	1.80
Apr	0.963	0.010	1.06
May	0.943	0.021	2.21
Jun	0.897	0.024	2.66
Jul	0.818	0.034	4.21
Aug	0.760	0.033	4.32
Sep	0.804	0.038	4.76
Oct	0.900	0.031	3.38
Nov	0.918	0.036	3.86
Dec	0.913	0.035	3.86

Monthly Trend Analysis

There was no statistically significant trend identified for ten of twelve calendar months with either the OLS or Mann–Kendall tests (Table 3; Figure 4). Under the nominal, uncorrected, significance level ($\alpha = 0.05$), there was an apparent decrease at three months: under Sen's slope, August (Sen's slope = −0.0385 MJ m−2 day−1 yr−1); September (Sen's slope = −0.0370; MK p = 0.036); and July (Sen's slope = −0.0455; OLS p = 0.017), although the latter month was only marginally significant under MK alone (with no correction for small, but present, lag-1 autocorrelation, p = 0.072). None of these three months, however, remained significant once the FDR or Bonferroni correction for the twelve-monthly tests was applied (Table 3), so this apparent decrease should be described as a nominally significant, uncorrected signal rather than as a robust, multiple-testing-adjusted trend.

The August and September decreases were not significant with the Bonferroni correction for the 12 monthly tests (adjusted p = 0.118 and 0.358, respectively), and they had the lowest adjusted p-values using the Benjamini-Hochberg FDR technique (0.100 and 0.119, respectively). No noticeable trend (positive or negative) was observed in any month throughout the dry season.

Correlation Between Solar Radiation and Climatic Drivers

Air temperature (T2M) and wind speed (WS2M) were highly positively correlated with solar radiation (Pearson r = 0.758 and 0.609; both p < 0.001),

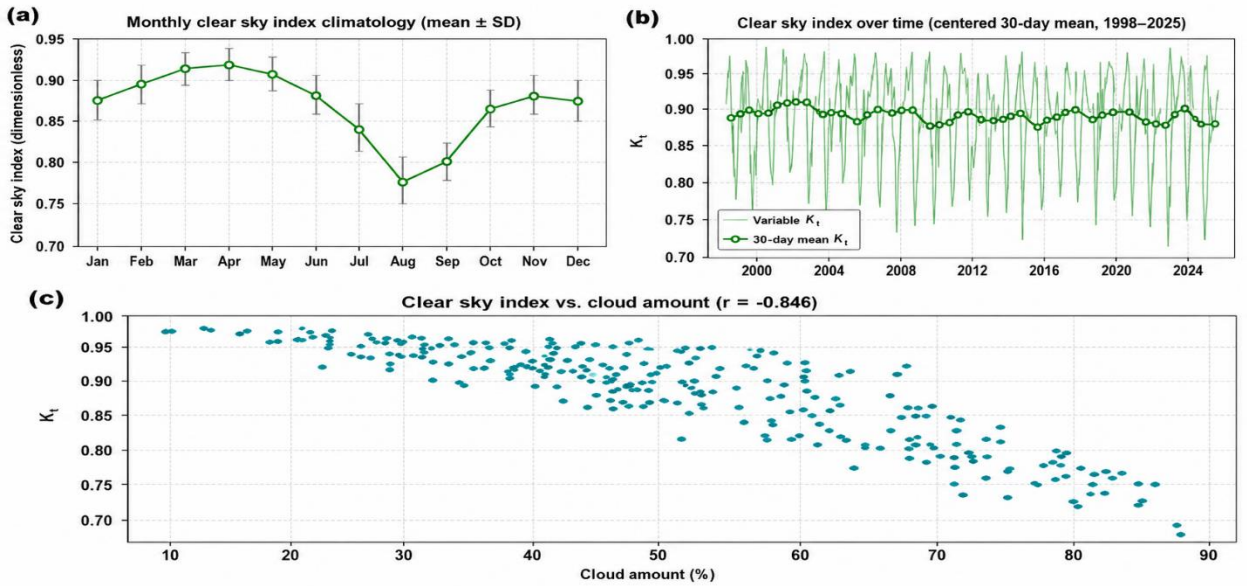


Figure 3. Clear-sky index (Kc) characteristics at the study grid point, 1998–2025. (a) Monthly Kc climatology (mean ± SD); (b) Kc over time, shown as the raw monthly series with a centred 30-day mean; (c) Kc versus cloud amount, showing the strong negative association (r = −0.846) underlying the cloud-attenuation relationship discussed in the text.

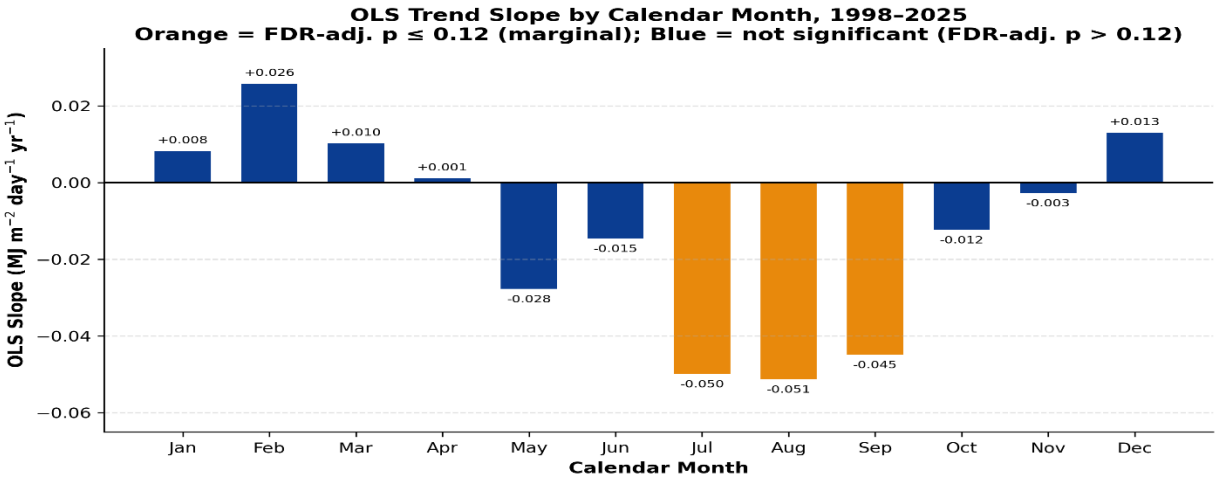


Figure 4. Monthly ordinary-least-squares (OLS) trend slope of solar radiation, 1998–2025, colour-coded by Benjamini–Hochberg FDR-adjusted significance (12 monthly tests). Orange bars (July, August, September) indicate FDR-adjusted p ≤ 0.12 (marginal); blue bars indicate FDR-adjusted p > 0.12 (not significant). No month remains significant at the conventional α = 0.05 threshold once corrected for multiple testing (**s**ee Table 3).

and cloud amount, specific humidity, and precipitation were negatively correlated with it (r = −0.348, −0.315, and −0.369; all p < 0.001) (Table 4; Figure 5). The associations between de-seasonalized T2M and WS2M were not significant (anomaly r = 0.019 and 0.024; p > 0.6).

The most robust negative relationship at the anomaly level was between cloud amount and solar radiation (anomaly r = −0.624, p < 0.001). Specific humidity and precipitation showed relatively strong, but small, negative anomaly correlations (r = −0.146 and −0.233; p < 0.01).

Multiple Regression and Relative Contribution of Climatic Drivers

The raw-value regression model accounted for a large amount of variance (R^2 = 0.788, F (5,329) = 245.2, p < 0.001) but had positive residual autocorrelation (Durbin–Watson = 1.02) and high multicollinearity for QV2M (VIF = 7.67) and WS2M (VIF = 4.08) (Table 5, Figure 6, Figure 7a-c).

Table 3. Trend statistics for solar radiation (ALLSKY_SFC_SW_DWN) by calendar month, 1998–2025, including both the standard and autocorrelation-corrected (modified Hamed–Rao) Mann–Kendall tests, with multiple-comparisons-corrected (OLS-based) p-values.

Month	OLS Slope	OLS p	MK Trend	MK p	Sen's Slope	FDR-adj. p	Bonferroni p	Mod. MK Trend	Mod. MK p
Jan	0.0082	0.692	no trend	0.489	0.0118	0.831	1.000	no trend	0.489
Feb	0.0258	0.250	no trend	0.072	0.0265	0.599	1.000	no trend	0.072
Mar	0.0102	0.654	no trend	0.767	0.0094	0.831	1.000	no trend	0.767
Apr	0.0011	0.948	no trend	0.874	0.0022	0.948	1.000	no trend	0.862
May	−0.0277	0.225	no trend	0.186	−0.0300	0.599	1.000	no trend	0.186
Jun	−0.0146	0.388	no trend	0.429	−0.0145	0.753	1.000	no trend	0.429
Jul	−0.0499	0.017	no trend	0.072	−0.0455	0.100	0.200	decreasing	0.006
Aug	−0.0513	0.010	decreasing	0.027	−0.0385	0.100	0.118	decreasing	0.027
Sep	−0.0449	0.030	decreasing	0.036	−0.0370	0.119	0.358	decreasing	0.036
Oct	−0.0123	0.502	no trend	0.693	−0.0051	0.753	1.000	no trend	0.693
Nov	−0.0027	0.901	no trend	0.890	−0.0023	0.948	1.000	no trend	0.890
Dec	0.0130	0.501	no trend	0.206	0.0282	0.753	1.000	no trend	0.206

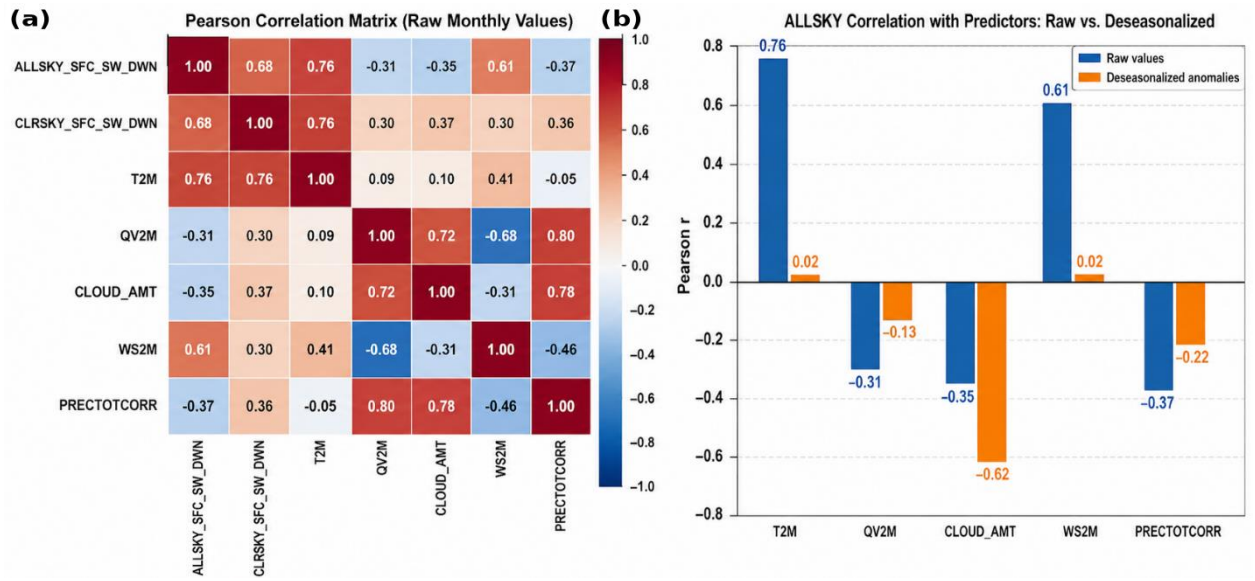


Figure 5. Correlation structure between solar radiation and candidate climatic drivers: (a) Pearson correlation matrix among all variables (raw monthly values); (b) ALLSKY_SFC_SW_DWN correlation with each candidate predictor, raw monthly values versus de-seasonalized anomalies.

Table 4. Pearson and Spearman correlation coefficients between solar radiation and climatic variables: raw monthly values vs. de-seasonalized anomalies.

Variable	Pearson r (raw)	p (raw)	Spearman r (raw)	p (raw)	Pearson r (anom.)	p (anom.)	Spearman r (anom.)	p (anom.)
T2M	0.758	<0.001	0.749	<0.001	0.019	0.724	0.021	0.708
QV2M	−0.315	<0.001	−0.264	<0.001	−0.146	0.008	−0.146	0.007
CLOUD_AMT	−0.348	<0.001	−0.308	<0.001	−0.624	<0.001	−0.634	<0.001
WS2M	0.609	<0.001	0.590	<0.001	0.024	0.664	0.009	0.874
PRECTOTCORR	−0.369	<0.001	−0.378	<0.001	−0.233	<0.001	−0.288	<0.001

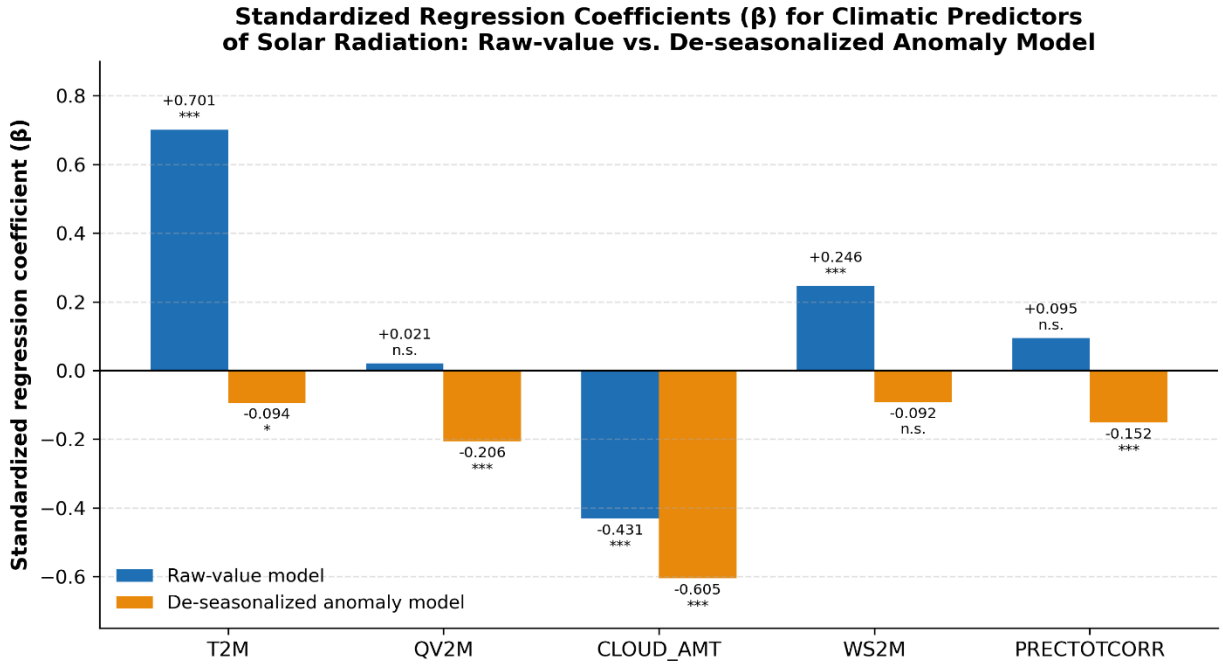


Figure 6. Standardized regression coefficients (β) for climatic predictors of solar radiation: raw-value model versus de-seasonalized anomaly model.

Table 5. Multiple regression results for solar radiation: raw-value model vs. de-seasonalized (anomaly) model.

Variable	Raw b	Raw SE	Raw p	Raw β	Raw VIF	Anom. b	Anom. SE	Anom. p	Anom. β	Anom. VIF
Constant	3.486	0.661	<0.001	—	—	0.002	0.035	0.964	—	—
T2M	0.656	0.034	<0.001	0.701	2.08	−0.094	0.045	0.036	−0.094	1.17
QV2M	0.009	0.031	0.767	0.021	7.67	−0.150	0.039	<0.001	−0.206	1.67
CLOUD_AMT	−0.056	0.006	<0.001	−0.431	3.03	−0.054	0.004	<0.001	−0.605	1.02
WS2M	0.893	0.186	<0.001	0.246	4.08	−0.353	0.200	0.079	−0.092	1.58
PRECTOTCORR	0.060	0.032	0.065	0.095	4.09	−0.108	0.030	<0.001	−0.152	1.06

Note. Raw model: $R^2 = 0.788$, $F(5,329) = 245.2$, $p < 0.001$, Durbin–Watson = 1.02. Anomaly model: $R^2 = 0.438$, $F(5,329) = 51.4$, $p < 0.001$, Durbin–Watson = 1.53.

Table 6. OLS vs. HAC (Newey–West, 12 lags) corrected standard errors and significance for both regression models.

Variable	Raw OLS p	Raw HAC p	Anom. OLS p	Anom. HAC p	Inference
T2M	<0.001	<0.001	0.036	0.068	Robust (raw); sensitive (anomaly)
QV2M	0.767 (n.s.)	0.831 (n.s.)	<0.001	0.002	Robust
CLOUD_AMT	<0.001	<0.001	<0.001	<0.001	Robust
WS2M	<0.001	<0.001	0.079 (n.s.)	0.186 (n.s.)	Robust
PRECTOTCORR	0.065 (n.s.)	0.038 (sig.)	<0.001	<0.001	Sensitive (raw); robust (anomaly)

Note. HAC = heteroscedasticity- and autocorrelation-consistent (Newey–West) standard errors, computed with 12 lags. "Sensitive" indicates the variable's significance classification (at α = 0.05) changes between the naive OLS and HAC-corrected estimates.

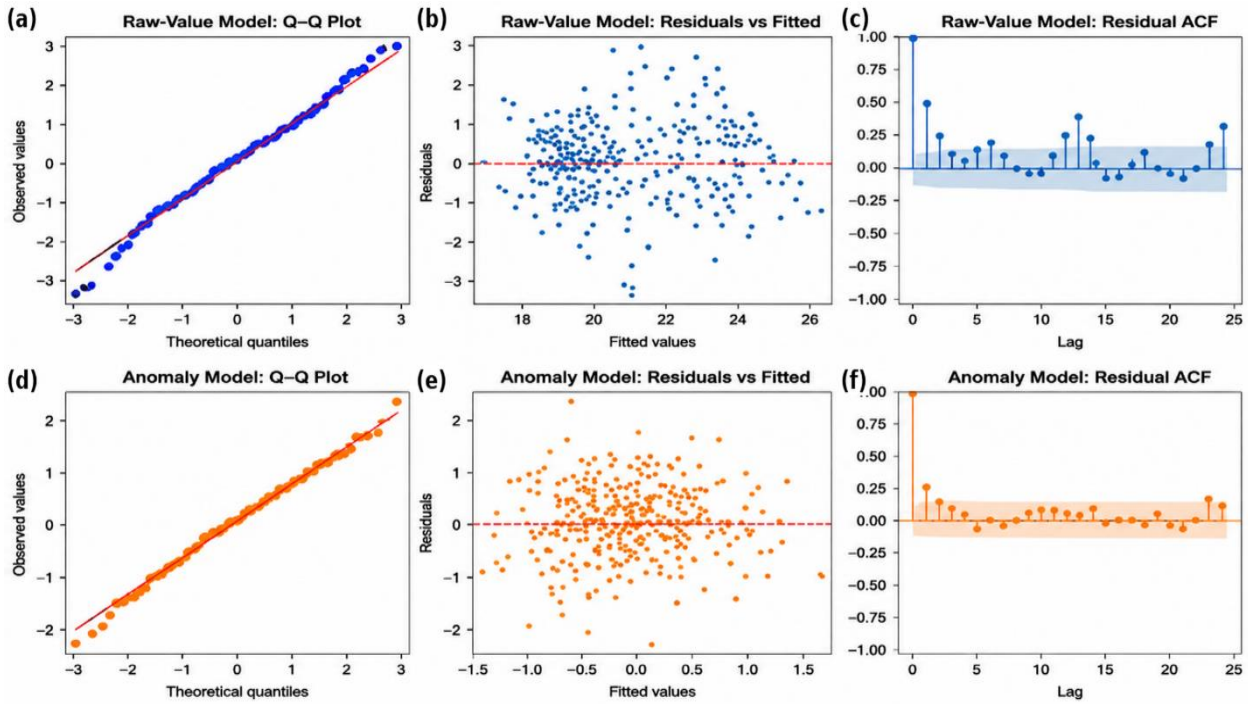


Figure 7. Residual diagnostics for the raw-value (a–c) and de-seasonalized anomaly (d–f) regression models: quantile–quantile plots (a, d), residuals vs. fitted values (b, e), and residual autocorrelation function (c, f).

In the de-seasonalized anomaly model (R^2 = 0.438, F (5,329) = 51.4, $p < 0.001$, Durbin–Watson = 1.53, all VIF < 1.7), cloud amount was the strongest predictor (standardized $\beta = -0.605$, $p < 0.001$), followed by specific humidity ($\beta = -0.206$, $p < 0.001$), precipitation ($\beta = -0.152$, $p < 0.001$), and temperature ($\beta = -0.094$, $p = 0.036$). Wind speed was not significantly associated in this model ($p = 0.079$).

Residual diagnostics for the de-seasonalized anomaly model (Figure 7d-f) showed no evidence of heteroscedasticity (Breusch–Pagan and White tests, both $p > 0.4$) and residuals consistent with normality (Shapiro–Wilk, $p = 0.251$), although a Ljung–Box test still detected residual autocorrelation ($p < 0.01$ at all tested lags); under HAC-corrected standard errors (Table 6), temperature's significance in this model is not robust (HAC $p = 0.068$, versus naive $p = 0.036$), and is interpreted with corresponding caution.

Solar Resource Climatology and Atmospheric Transmissivity in Regional Context

At the studied grid point, solar resource availability was high and relatively stable for approximately seven months of the year, according to the 28-year climatology. From November to May, surface irradiance tracked 90–96% of its theoretical clear-sky ceiling, with clear-sky index (Kc) values of 0.90–0.96. This range is comparable to the values obtained from other Sahelian and Sudano-Sahelian sites, where the ITCZ moves southward during the dry season, allowing the region to be under the influence of the dry, dusty, but often cloud-free Harmattan flow [22]. The rapid drop in Kc in the monsoon core (with a minimum Kc in August, 0.760) and the near quadrupling of the coefficient of variation of Kc compared to the dry season is now a pattern well observed throughout the Sahelian and sub-Sahelian belt in West Africa. In the Sahel, where the ITCZ is at its peak seasonal location, [22] showed that cloud-induced attenuation of incoming shortwave radiation is at its peak in August, with typical values of 20–35% compared to the ITCZ in clear-sky conditions. This is even higher along the Guinea coast, where the ITCZ is found in August. The ITCZ-modulated seasonality of atmospheric transmissivity is a dominant factor for the solar climatology of West Africa rather than a site-specific anomaly, as evidenced by the August/September minimum reported here for The Gambia, a region with transitional climatic characteristics between the coastal humid fringe and the Sahelian dry interior.

This seasonal signature is also consistent with satellite- and reanalysis-based evidence that low-level, non-precipitating stratiform clouds, which are not a major rainfall-producing system in the Sahel, cover the southern and central sub-region in the core monsoon months and cause shortwave attenuation mainly during the day, regardless of precipitation

intensity [23]. The physical reason that this minimum in the clear sky index does not always occur at the same time as the precipitation maximum, but rather at the same time as the minimum in Kc for the present record, is that the low-level cloud systems are not necessarily tied to the diurnal precipitation cycle.

Temporal Trends in Solar Radiation: Absence of a Robust Long-Term Signal

The results showed that 10 of the 12 calendar months had no statistically significant trend, while the two months that showed nominally significant trends (August and September), both indicating dimming rather than brightening, did not remain significant once the Bonferroni correction for multiple comparisons was applied. This suggests that the solar radiation record for Gambia from 1998 to 2025 is best described as stable rather than systematically dimming or brightening. Studies on global dimming and brightening have shown that the global signal does not necessarily remain constant on multi-decadal timescales; in many cases, surface shortwave radiation (SW) decreased significantly in the period 1950–1980, then increased somewhat, with the change primarily caused by variations in aerosol loading and secondarily by changes in cloud properties [24-26]. The absence of a comparable directional signal in the present record from Gambia does not conflict with this work; it simply indicates that the anthropogenic aerosol forcing that is known to produce a signal of such type as is evident in mid-latitude and East Asian records did not result in a detectable equivalent signature at this Sahelo-Sudanian site during the study period, or that any such signal is not detectable in a single-grid-point, 28-year monthly series after correction for multiple testing.

It is noteworthy that the lowest (although still non-significant) adjusted p-values were observed during August and September. The near-surface temperature rise and cloud frequency rise are two factors that contribute to the projected reduction in solar resources or photovoltaic potential in West Africa in the coming decades, with the months affected by the monsoon and the more humid areas being more exposed ([27-29]. The preliminary monsoon-season drop found in this study, although not statistically significant after correction for multiple comparisons, is in the same direction as the monsoon-season drop expected for the region given continued climate change and should be monitored over time as the data record lengthens; a longer observational record, rather than an extrapolation of the current slope estimates, will be required to establish whether this pattern is a genuine, detectable trend.

Climatic Drivers of Solar Radiation Variability: Disentangling Seasonality from Weather-Scale Coupling

The most significant result of the study was the difference between the raw and de-seasonalized correlation structures, which was best understood. Monthly all-weather values of air temperature and wind speed showed the highest positive correlations with solar radiation ($r = 0.758$ and 0.609, respectively), whereas cloud cover, humidity, and precipitation were negatively correlated. After the common annual cycle was removed, however, the correlations between temperature and wind speed became statistically insignificant ($r = 0.019$ and 0.024, respectively; Table 4), while the correlation between cloud cover remained the highest at the anomaly level ($r = -0.624$), and humidity and precipitation showed modest but statistically significant negative correlations. This pattern indicates that, in large part, the raw-value correlations between temperature and wind speed were a statistical artifact of the synchronized seasonal cycles of both variables, such that both increased during the warm, dry season, for reasons unrelated to a direct radiative influence of one variable on the other.

This distinction is in line with the physical understanding of the modulation of the shortwave radiation flux by the atmosphere, which has been established in a larger body of dimming and brightening studies, and where it is found that cloud cover and its optical properties are the principal modulators on sub-decadal and interannual timescales, while other components of the atmosphere, such as aerosol and water-vapor loading, are secondary [26, 30]. The negative cloud–radiation correlation (CRA) coefficient after deseasonalization shows that the intra-seasonal (weather-scale) variation in cloudiness (such as the passage of individual mesoscale convective systems or transient low-level stratiform cloud episodes during the monsoon) has an effect on solar radiation that is separate from and in addition to the seasonal cycle itself.

Cloud Cover as the Dominant Driver: Regression Evidence and Multicollinearity Considerations

The multiple regression results confirm and expand the correlation findings. The high R^2 (0.788) is linked with significant multicollinearity (VIF of specific humidity = 7.67, VIF of wind speed = 4.08), such as the seasonality shared by the predictors and positive residual autocorrelation (Durbin–Watson = 1.02), which suggests some caution should be used when interpreting the standard errors and the apparent dominance of temperature (standardized β = 0.701) in this model, consistent with established guidance on interpreting regression coefficients when variance inflation is high [20]. The de-seasonalized anomaly model, on the other hand, has very good residual behaviour (Durbin–Watson = 1.53) with no noticeable multicollinearity (all VIF < 1.7) and is thus a more credible building block for attributing relative importance to the predictors. For this model, the cloud amount is the largest contributor to the solar radiation variability by a considerable margin (standardized β = −0.605), followed at considerably lower magnitude by specific humidity (β = −0.206), precipitation (β = −0.152), and temperature (β = −0.094); wind speed is not a significant predictor (p = 0.079).

The ranking is well supported by the literature in West Africa on the physical controls of surface solar radiation. The cloud shortwave attenuation research conducted by both the CERES satellite observations and ERA5 reanalysis consistently shows that total and low-level cloud fraction are the main modulators of incoming solar radiation in the Sahelian and Sudanian zones, with the amplitude of the cloud shortwave attenuation closely linked to the seasonal and sub-seasonal evolution of cloud cover rather than to the temperature and wind fields [23,31]. The relative importance of specific humidity and precipitation in the anomaly model is also like the relative importance of cloud amount, which is also found to be partly collinear, implying the presence of an atmospheric moisture pathway to cloud formation but not necessarily of a radiative pathway of comparable strength. The raw-value association with solar radiation is apparently due to the common enhancement of both variables during the dry season as the Harmattan increases, rather than a direct effect at the monthly timescale (as might be seen in a mechanism such as boundary-layer mixing or aerosol dispersal), because of the loss of this association following removal of the seasonal cycle.

Implications for Solar Energy Planning and Policy in The Gambia

The implications of these findings are apparent for the renewable energy goals stated in the introduction. The persistently high and relatively stable Kc observations from November to May are consistent with a dry-season solar resource at this representative Gambian grid point that is comparable in overall quality with other high-insolation regions in West Africa, lending general support to the premise that the dry season is favourable for solar deployments in the country, including planned grid-connected photovoltaic (PV) utility-scale capacity such as that proposed for Kombo South; confirming the site-specific adequacy of any particular project location, however, would require dedicated, higher-resolution assessment beyond the scope of this single, coarse-resolution grid-point climatology. This aligns with the monthly solar irradiation estimates from independent ground-based observations at the Yundum and Basse meteorological stations, which range broadly across both stations and are generally interpreted as indicating a resource favourable for both grid and off-grid PV systems, though system-level sufficiency ultimately depends on additional engineering, demand, and storage considerations not evaluated here [32]. The present analysis adds to this evidence base by identifying cloud cover, rather than temperature or wind, as the variable most strongly associated with month-to-month variability in surface solar radiation at this site. This association-based finding suggests, though does not by itself demonstrate, that cloud-focused nowcasting (forecasting for the next hour or day) may be a more informative basis for short-term solar radiation forecasting in the country than temperature-based heuristics, and that seasonal cloud variability is a relevant factor for forecasting and storage-planning efforts to take into account; translating this irradiance-based association into specific forecasting or battery-storage-sizing parameters would require dedicated forecasting and system-modelling studies beyond the scope of the present climatological analysis, consistent in direction with other cloudiness-based solar energy management findings in West Africa [23].

The monsoon-season depression in transmissivity is relatively small compared to the dry-season baseline, but it has a compounding implication for the planning of the grid: it is the period of the year when transmissivity variability is highest due to cloud cover

(Table 1) and, based on the trend analysis, it is the time of the year when some (statistically tentative) degradation in resource quality already might be occurring. In light of the regional, CMIP6-derived projections of a likely expansion of the solar deficit in West Africa in the coming century (mostly in the June–August period) [33], and given that the present, site-specific trend evidence remains statistically inconclusive after correction for multiple comparisons, energy planners in The Gambia may wish to treat the current monsoon-season solar deficit as a lower bound rather than a fixed design constraint when planning energy projects, and to consider a margin for a possible future increase, particularly for projects with operational lifetimes of decades or more; this recommendation follows primarily from the cited regional projections rather than from a statistically robust trend detected in the present dataset. Satellite-based solar resource assessments over multi-decadal records have further highlighted the need for historical characterization of solar resources for reliable long-term yield estimation for both utility-scale and off-grid systems [34], underscoring the relevance of this present climatology as one input, among others, for future solar energy planning and investment appraisal in West Africa.

Study Limitations and Directions for Future Research

The above interpretation should be understood in the context of the methodological limitations discussed below. Most fundamentally, this study is based on a single coarse-resolution (~50–60 km) grid point and therefore cannot resolve any coastal-to-inland or riverine microclimatic gradients that may exist across the country. Although The Gambia's narrow latitudinal range (<1°) suggests that such gradients may be modest, this cannot be confirmed without a national network of ground-based or multi-point satellite-derived observations, which does not currently exist for the country [35]. The findings presented here should, therefore, be interpreted as characteristic of this specific central location rather than as spatially representative of the whole of The Gambia. Second, the retained residual autocorrelation of the raw-value regression model (Durbin–Watson = 1.02) indicates that climatic time series of this type have some degree of dependence that remains after the predictors are included, and explicit autoregressive or generalized least-squares models would be welcome in future studies. Third, the non-parametric trend tests used here are conservative in a 28-year data record and should be revisited with a longer data record; they would also be better validated with independent satellite cloud products such as those employed in regional cloud-attenuation studies [23,31], to get a clearer idea of whether the signal is real or spurious. Finally, the present analysis is restricted to monthly mean statistics and cannot directly test this physical mechanism because it is this type of cloud anomaly radiation coupling that is most likely to produce the strong cloud radiation anomaly coupling documented here, but only at a sub-monthly event scale. A higher-frequency follow-up analysis could incorporate cloud-type classification to test this coupling directly rather than by inference from monthly statistics.

Conclusion

This study provides a point-scale assessment of solar resource availability and its climatic drivers at a representative central grid point in The Gambia over the last 28 years (1998–2025), contributing to a long-term, multivariable dataset for solar energy characterization at this location. The findings confirm that, at this grid point, November to May has a high and relatively stable solar resource, similar to the rest of the high-insolation part of the Sahelo-Sudanian belt (Kc = 0.90–0.96), whereas the monsoon core (July–September) is defined by significantly lower and more variable solar resource (Kc = 0.760 at the lowest in August). A long-term trend analysis showed no statistically significant change in solar radiation during the study period, suggesting that this resource has not changed significantly over time, albeit with some small, nominally significant (but not multiple-testing-corrected) decreases in August and September, which should be monitored in the future as the observation period increases. Overall, once multiple comparisons are properly accounted for, the solar radiation resource at this grid point is best described as stable rather than declining.

The strong raw-value correlation and regression with air temperature and wind speed were mainly seasonal artifacts and did not suggest direct physical coupling, as the relationship between solar radiation and both air temperature and wind speed was not statistically significant after de-seasonalisation. In contrast, cloud amount proved to be the most important and physically strong parameter for both the seasonal and intra-seasonal variations of solar radiation, while specific humidity and precipitation played secondary and partly co-linear roles.

The results obtained from the de-seasonalised model are more statistically defensible and confirm that cloud dynamics is the main atmospheric control over surface solar radiation availability in The Gambia, as is generally reported in the West African literature on cloud-modulated shortwave attenuation.

Collectively, these findings are consistent with a favourable solar radiation resource for solar energy development at this representative Gambian location, especially in the dry season, and indicate that the seasonal variation of cloud cover and associated atmospheric attenuation is a factor that solar forecasting, storage planning, and long-term system design efforts in The Gambia should take into account, though translating this resource characterization into specific forecasting, storage, or design parameters would require dedicated engineering and economic analysis beyond the scope of this study. This study was based entirely on a single coarse-resolution grid point, and there was no ground-based radiometric validation. For future studies, more detailed and frequent observations, in situ pyranometric validation data, and longer time series are needed to improve the ability to detect trends and to better support the empirical basis for long-term solar energy planning and policy formulation across The Gambia, building outward from this single-site baseline.

Data and Code Availability

Data availability

Monthly climate data for the study grid point (13.45° N, 15.38° W) used to support the findings of this study are publicly available and freely accessible without any restrictions or registration requirements from the NASA Prediction of Worldwide Energy Resources (POWER) Data Access Viewer (https://power.larc.nasa.gov/data-access-viewer/).

Code availability

Python code used for data processing, statistical analysis (Mann–Kendall trend testing, Theil-Sen slope estimation, Pearson-Spearman correlation, OLS regression, VIF and Durbin-Watson diagnostics, and Benjamini-Hochberg/Bonferroni multiple-testing correction), and visualization is available from the corresponding author upon reasonable request.

Acknowledgements

The authors gratefully acknowledge the National Aeronautics and Space Administration (NASA) for providing open access to the Prediction of Worldwide Energy Resources (POWER) dataset, which formed the basis of this study. The authors also appreciate the developers of the open-source Python scientific computing libraries used for data processing, analysis, and visualization.

References

[1] D. Gielen, F. Boshell, D. Saygin, M.D. Bazilian, N. Wagner, R. Gorini, The Role of Renewable Energy in the Global Energy Transformation, Energy Strateg. Rev. **24** (2019) 38–50. DOI: 10.1016/j.esr.2019.01.006.

[2] O.O. Apeh, E.L. Meyer, O.K. Overen, Contributions of Solar Photovoltaic Systems to Environmental and Socioeconomic Aspects of National Development—A Review, Energies. **15** (2022) 5963. DOI: 10.3390/en15165963.

[3] K. Ukoba, K.O. Olatunji, E. Adeoye, T.-C. Jen, D.M. Madyira, Optimizing Renewable Energy Systems Through Artificial Intelligence: Review and Prospects, Energy Environ. **35** (2024) 3833–3879. DOI: 10.1177/0958305X241256293.

[4] L.K. Marong, S. Jirakiattikul, K. Techato, The Gambia's Future Electricity Supply System: Optimizing Power Supply for Sustainable Development, Energy Strateg. Rev. **20** (2018) 179–194. DOI: 10.1016/j.esr.2018.03.001.

[5] N.A. Obeng-Darko, Renewable energy development in sub-Saharan Africa: Evidence of Regulatory Issues From The Gambia and Nigeria, Renew. Energy Law Policy Rev. **9** (2020) 36–44. DOI: 10.4337/relp.2020.04.04.

[6] H. Jin, S. Wang, P. Yan, L. Qiao, L. Sun, L. Zhang, Spatial and Temporal Characteristics of Surface Solar Radiation in China and its Influencing Factors, Front. Environ. Sci. **10** (2022) 916748. DOI: 10.3389/fenvs.2022.916748.

[7] J. Bai, X. Zong, Global Solar Radiation Transfer and Its Loss in the Atmosphere, Appl. Sci. **11** (2021) 2651. DOI: 10.3390/app11062651.

[8] W. Mol, B. Heusinkveld, M.R. Mangan, O. Hartogensis, M. Veerman, C. Van Heerwaarden, Observed Patterns of Surface Solar Irradiance under Cloudy and Clear-sky Conditions, Q. J. R.

Meteorol. Soc. **150** (2024) 2338–2363. DOI: 10.1002/qj.4712.

[9] A.K. Shrestha, A. Thapa, H. Gautam, Solar Radiation, Air Temperature, Relative Humidity, and Dew Point Study: Damak, Jhapa, Nepal, Int. J. Photoenergy. **2019** (2019) 1–7. DOI: 10.1155/2019/8369231.

[10] N.A. Ibrahim, S.R. Wan Alwi, Z. Abd Manan, A.A. Mustaffa, K. Kidam, Climate Change Impact on Solar System in Malaysia: Techno-economic Analysis, Renew. Sustain. Energy Rev. **189** (2024) 113901. DOI: 10.1016/j.rser.2023.113901.

[11] N. Duque-Gardeazabal, S. Brönnimann, A.R. Friedman, E. Dolores-Tesillos, O. Martius, Solar and Wind Energy Variability in Tropical South America: Seasonal Ocean-Atmospheric Modulators, Meteorol. Appl. **33** (2026) e70165. DOI: 10.1002/met.70165.

[12] A. Kniffka, P. Knippertz, A.H. Fink, The Role of Low-level Clouds in the West African Monsoon System, Atmos. Chem. Phys. **19** (2019) 1623–1647. DOI: 10.5194/acp-19-1623-2019.

[13] L. Clauzel, S. Anquetin, C. Lavaysse, G. Bergametti, C. Bouet, G. Siour, R. Lapere, B. Marticorena, J. Thomas, Solar Radiation Estimation in West Africa: Impact of Dust Conditions During the 2021 Dry Season, Atmos. Chem. Phys. **25** (2025) 997–1021. DOI: 10.5194/acp-25-997-2025.

[14] H. Tao, I. Ebtehaj, H. Bonakdari, S. Heddam, C. Voyant, N. Al-Ansari, R. Deo, Z.M. Yaseen, Designing a New Data Intelligence Model for Global Solar Radiation Prediction: Application of Multivariate Modeling Scheme, Energies. **12** (2019) 1365. DOI: 10.3390/en12071365.

[15] Y. Choi, J. Suh, S.-M. Kim, GIS-Based Solar Radiation Mapping, Site Evaluation, and Potential Assessment: A Review, Appl. Sci. **9** (2019) 1960. DOI: 10.3390/app9091960.

[16] A.D. Quansah, F. Dogbey, P.J. Asilevi, P. Boakye, L. Darkwah, S. Oduro-Kwarteng, Y.A. Sokama-Neuyam, P. Mensah, Assessment of Solar Radiation Resource from the NASA-POWER Reanalysis Products for Tropical Climates in Ghana Towards Clean Energy Application, Sci. Rep. **12** (2022) 10684. DOI: 10.1038/s41598-022-14126-9.

[17] R.M. Da Silva, C.A.G. Santos, M. Moreira, J. Corte-Real, V.C.L. Silva, I.C. Medeiros, Rainfall and River Flow Trends using Mann–Kendall and Sen's slope Estimator Statistical Tests in the Cobres River Basin, Nat. Hazards. **77** (2015) 1205–1221. DOI: 10.1007/s11069-015-1644-7.

[18] S.M. Ahmed, Assessment of Irrigation System Sustainability using the Theil–Sen Estimator of Slope of Time Series, Sustain. Sci. **9** (2014) 293–302. DOI: 10.1007/s11625-013-0237-1.

[19] Y. Benjamini, Y. Hochberg, Controlling the False Discovery Rate: A Practical and Powerful Approach to Multiple Testing, J. R. Stat. Soc. Ser. B Stat. Methodol. **57** (1995) 289–300. DOI: 10.1111/j.2517-6161.1995.tb02031.x.

[20] R.M. O'Brien, A Caution Regarding Rules of Thumb for Variance Inflation Factors, Qual. Quant. **41** (2007) 673–690. DOI: 10.1007/s11135-006-9018-6.

[21] J. Durbin, G.S. Watson, Testing for Serial Correlation in Least Squares Regression. III, Biometrika. **58** (1971) 1–19. DOI: 10.1093/biomet/58.1.1.

[22] D.K. Danso, S. Anquetin, A. Diedhiou, R. Adamou, Cloudiness Information Services for Solar Energy Management in West Africa, Atmosphere. **11** (2020) 857. DOI: 10.3390/atmos11080857.

[23] D.K. Danso, S. Anquetin, A. Diedhiou, K. Kouadio, A.T. Kobea, Daytime Low-level Clouds in West Africa – Occurrence, Associated Drivers, and Shortwave Radiation Attenuation, Earth Syst. Dyn. **11** (2020) 1133–1152. DOI: 10.5194/esd-11-1133-2020.

[24] S. Cohen, The Role of Widespread Surface Solar Radiation Trends in Climate Change, in: Climate Change, Elsevier, 2009, pp. 21–41. DOI: 10.1016/B978-0-444-53301-2.00002-6.

[25] P.J. Taylor, Natural Drivers of Global Warming: Ocean Cycles, Anthropogenic Greenhouse Gases and the Question of Percentages, J. Environ. Earth Sci. **7** (2025). DOI: 10.30564/jees.v7i2.7683.

[26] M. Wild, Global Dimming and Brightening: A review, J. Geophys. Res. Atmos. **114** (2009) 2008JD011470. DOI: 10.1029/2008JD011470.

[27] A. Bichet, B. Hingray, G. Evin, A. Diedhiou, C.M.F. Kebe, S. Anquetin, Potential Impact of Climate Change on Solar Resource in Africa for Photovoltaic Energy: Analyses from CordEX-Africa Climate Experiments, Environ. Res. Lett. **14** (2019) 124039. DOI: 10.1088/1748-9326/ab500a.

[28] A. Ndiaye, M.S. Moussa, C. Dione, W. Sawadogo, J. Bliefernicht, L. Dungall, H. Kunstmann, Projected Changes in Solar PV and Wind Energy Potential over West Africa: An Analysis of CORDEX-CORE Simulations, Energies. **15** (2022) 9602. DOI: 10.3390/en15249602.

[29] S. Obahoundje, A. Diedhiou, A. Troccoli, P. Boorman, T.A.F. Alabi, S. Anquetin, L. Crochemore, W.F. Fassinou, B. Hingray, D. Koné, C. Mamadou, F. Sorho, Teal-WCA: A Climate Services Platform for Planning Solar Photovoltaic and Wind Energy Resources in West and Central Africa in the Context of Climate Change, Data. **9** (2024) 148. DOI: 10.3390/data9120148.

[30] Y. Jiang, B. Yi, An Assessment of the Influences of Clouds on the Solar Photovoltaic Potential over China, Remote Sens. **15** (2023) 258. DOI: 10.3390/rs15010258.

[31] D.K. Danso, S. Anquetin, A. Diedhiou, C. Lavaysse, A. Kobea, N.E. Touré, Spatio-temporal Variability of Cloud Cover Types in West Africa with Satellite-based and Reanalysis data, Q. J. R. Meteorol. Soc. **145** (2019) 3715–3731. DOI: 10.1002/qj.3651.

[32] T.J. Ayua, O.T. Uto, L.K.M. Fatty, An Investigation of Solar Energy Potential Towards Improving Agriculture using Angstrom and Newly Developed Analytical Models: In the case of The Gambia, Sci. Afr. **21** (2023) e01886. DOI: 10.1016/j.sciaf.2023.e01886.

[33] D.K. Danso, S. Anquetin, A. Diedhiou, C. Lavaysse, B. Hingray, D. Raynaud, A.T. Kobea, A CMIP6 Assessment of the Potential Climate Change Impacts on Solar Photovoltaic Energy and its Atmospheric Drivers in West Africa, Environ. Res. Lett. **17** (2022) 044016. DOI: 10.1088/1748-9326/ac5a67.

[34] I. Neher, S. Crewell, S. Meilinger, U. Pfeifroth, J. Trentmann, Photovoltaic Power Potential in West Africa using Long-term Satellite Data, Atmos. Chem. Phys. **20** (2020) 12871–12888. DOI: 10.5194/acp-20-12871-2020.

[35] A.D. Quansah, F. Dogbey, P.J. Asilevi, P. Boakye, L. Darkwah, S. Oduro-Kwarteng, Y.A. Sokama-Neuyam, P. Mensah, Assessment of Solar Radiation Resource from the NASA-POWER Reanalysis Products for Tropical Climates in Ghana Towards Clean Energy Application, Sci. Rep. **12** (2022) 10684. DOI: 10.1038/s41598-022-14126-9.